This is a peer-reviewed, author's accepted manuscript of the following research article: Maclure, D. M., Chen, C., McKendry, J. J. D., Xie, E., Hill, J., Herrnsdorf, J., Gu, E., Haas, H., & Dawson, M. D. (Accepted/In press). Hundred-meter Gb/s deep ultraviolet wireless communications using AlGaN micro-LEDs. *Optics Express*.

Hundred-Meter Gb/s Deep Ultraviolet Wireless Communications using AlGaN Micro-LEDs

DANIEL M. MACLURE[1†], CHENG CHEN[2†], JONATHAN J.D. MCKENDRY[1†], ENYUAN XIE[1], JORDAN HILL[1], JOHANNES HERRNSDORF[1], ERDAN GU[1], HARALD HAAS[2], AND MARTIN D. DAWSON[1]

[1]*Institute of Photonics, Department of Physics, SUPA, University of Strathclyde, Glasgow G1 1RD, UK.*
[2]*LiFi Research and Development Centre, Department of Electronic & Electrical Engineering, The University of Strathclyde, Glasgow G1 1RD, UK.*

daniel.maclure@strath.ac.uk
c.chen@strath.ac.uk

Keywords: OFDM, Deep ultraviolet, Micro-LED, Optical Wireless Communications

Abstract: We demonstrate the use of deep ultraviolet (DUV) micro-LEDs for long-distance line-of-sight optical wireless communications. With a single 285nm-emitting micro-LED, we have respectively achieved data rates greater than 6.5 Gb/s at a distance of 10m and 4 Gb/s at 60m. Moreover, we obtained >1Gb/s data rates at a distance of 116 m. To our knowledge, these results are the highest data rates at such distances thus far reported using deep DUV micro-LEDs and the first demonstration of Gb/s communication at >100m using any micro-LED-based transmitter.

1. Introduction

Radio frequency (RF) communications technology is, on its own, unlikely to meet the ever-growing demand for wireless data transmission [1]. There is thus a move towards alternative communication systems such as optical wireless communications (OWC) [2] to complement the existing RF infrastructure. These new OWC systems utilize an additional license-free region of the EM spectrum and can also benefit communications applications in sectors such as defense [3] and financial services. In recent years, the extension of OWC to the deep ultraviolet (DUV, 200-315nm) has seen increased interest as the atmosphere attenuates and scatters DUV more strongly than at longer wavelengths [4,5]. As the upper atmosphere absorbs nearly all of the DUV region of the electromagnetic spectrum, it is a good candidate for secure inter-satellite communications as the signal is hidden from ground observers [6]. Moreover, this allows DUV terrestrial communications links to operate in a near noise-free environment [7]. Furthermore, due to the strong Rayleigh and Mie scattering of DUV by the atmosphere, it is possible to use DUV in a non-line-of-sight (NLOS) configuration [8,9]. Diffuse LOS and NLOS OWC could help overcome obstacles blocking the communication channel and relax constraints on pointing and tracking between transmitters and receivers [7]. Initial work in the DUV focused on low bandwidth mercury flash lamps, however, in recent years, high-quality UV lasers and light-emitting diodes (LEDs) have been developed, which provide new opportunities in DUV communications.

Micro-LEDs (µLEDs) are LED devices with active region a few microns to several 10's of microns in size. These devices are under intensive development for numerous applications [10], such as micro-displays [11] and small size, weight, and power (low SWaP) optical communications [12]. There are several benefits to using µLEDs in OWC, such as their reduced capacitance[13,14]. As a result, the carrier lifetime of the devices substantially defines the bandwidth, allowing for modulation bandwidths of many hundreds of MHz to above a GHz, compared to around 10 MHz for a conventional LED format [15]. This higher bandwidth is advantageous in communications, resulting in high data rates due to the resulting increased channel capacity [16]. In previous work, most µLED or LED OWC demonstrations were limited to distances of a few meters [6,17,18], with the research largely being focused on high data rate 'benchtop' systems using a variety of modulation techniques. Here, by optimizing a wide range of device and systems parameters, we demonstrate Gb/s data rates at >100m transmission distances using a single DUV µLED pixel with a peak emission wavelength of approximately 285 nm. Furthermore, we demonstrate the ability to transmit these high data rates with relatively low power (on the order of µWatts), and we demonstrate the ability of µLED communication systems to operate in ambient light (see Section 4). We also examine the effect of peak-to-peak voltage (VPP) and bit loading on the data rate. Finally, at all distances recorded we achieved Gb/s data rates and these results are, to our knowledge, the highest data rates at the longest distances reported using a single DUV µLED pixel.

2. Devices and Characterization

2.1 µLED Device Design and Fabrication

The device used in this work is an 8-segment concentric array of individually addressable trapezoidal-shaped µLEDs, each with an approximate active area of 1369 μm^2 (equivalent area to a circular pixel of diameter ~40 µm). The benefits and features of this pixel geometry were presented in previous publications [6,17,19]. Similarly, the device structure chosen was the same as described in [17], which had been previously shown empirically to be a pixel size and design that provided a good compromise between output power and modulation bandwidth. The devices are made from AlGaN-based LED epistructures grown on a c-plane sapphire substrate, the substrate being optically polished afterwards. The pixels were mesa etched, with individually addressable anodes and a shared cathode, and with an insulating layer surrounding the mesa. The pixels are configured to operate in a flip-chip configuration with the light emitted through the transparent sapphire substrate. The pixel has a six-period quantum well (QW) active region of AlGaN, the n-type layer comprises of 2µm-thick AlGaN, and the p-type layer consists of 310nm-thick p-doped GaN. Further details of the epi-structure are provided in our previous work [6].

2.2 µLED characterization

To measure the device's light output and current versus voltage (L-I-V) characteristics, the individual µLED pixels and an optical power meter were aligned in close proximity. We collected the light from the front of the device, i.e., from the sapphire substrate side, which is the format used in the communications setup described below. The optical power was measured using a calibrated optical power meter (Thorlabs PM100A) and sensor (S120VC), and the current and voltage were recorded using a Yokogawa GS610 Source-Measure Unit. The spectra were measured using a spectrometer (Aventes Avaspec-2048) and collection fiber-optic (Ocean Optics© QP600-2-SR-BX fiber). The modulation bandwidth was measured using an avalanche photodiode (APD, Hamamatsu C5668 8867 with a -3dB bandwidth of 1 GHz), two 2" lenses (Edmund Optics 84340) set around 19cm apart, and a network analyzer (PicoVNA 106, 300kHz-6GHz bandwidth) to record the frequency response. The bandwidth was estimated by measuring the frequency corresponding to a -3dB decrease from the 1 MHz point, as detailed in [17]. The L-I characteristic (Fig. 1. (a)) of a representative µLED pixel demonstrates a through-sapphire directed output power of around 0.4 mW at a current of 20 mA. The turn-on voltage (Fig. 1. (a)), around 7.8 V (at 1 mA current), is improved from our previous work but still shows effects of the poor electrical conductivity of AlGaN layers, an issue widely reported for DUV LEDs[20]. The L-I-V curve is used to help determine the optimum bias point of the μLED for the communications system demonstration (which uses direct current optical orthogonal frequency-division multiplexing, DCO-OFDM), as described in Section 3.

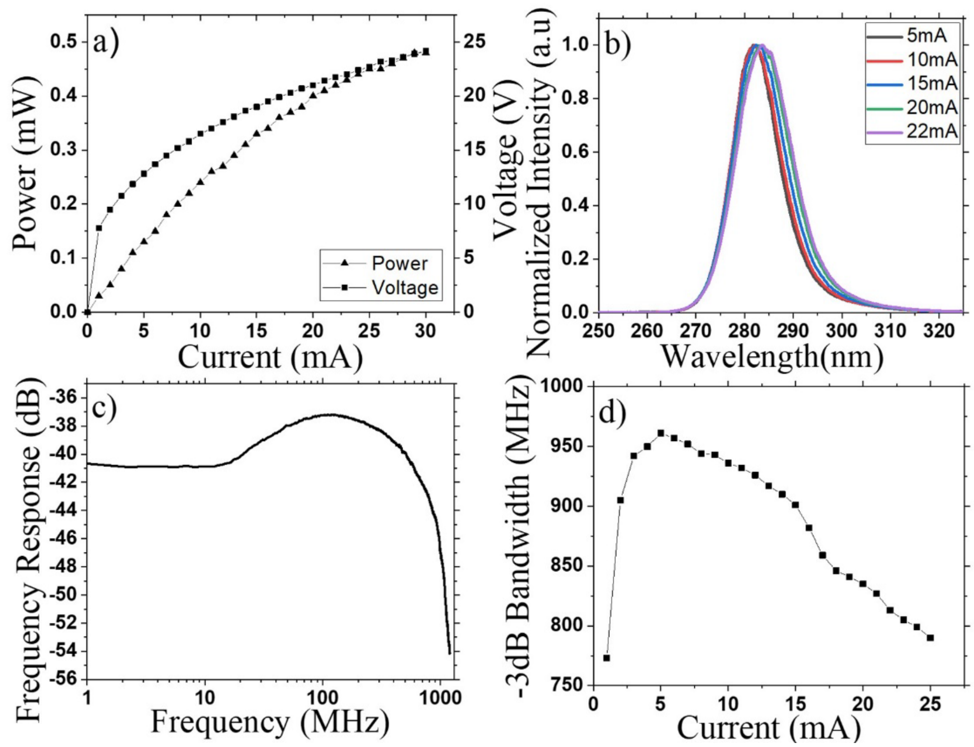

Fig. 1. Pertinent characteristics of the μLED pixels, a) LIV characteristics, b) normalized spectra for a range of drive currents c) Representative frequency response curve measured at 20mA and d) modulation bandwidth.

The μLED electroluminescence (EL) spectra versus current are shown in Fig. 1(b) for a representative single pixel. The μLED device has a peak emission wavelength of around 285 nm at 20 mA. The EL full width half maximum (FWHM) is approximately 10 nm, and as a result, the spectra cover part of both the UVB (280-315 nm) and UVC (100-280 nm) regions of the spectrum. The spectra of the μLEDs are relatively stable with current, with slight redshifts and small changes in the FWHM of the device, influenced by numerous factors such as band filling, field screening and thermal effects as observed in similar devices [21]. The small-signal frequency response measured at a bias of 20mA is shown in Fig. 1(c). This is the same bias as used to obtain the data transmission results as will be shown in Section 4. As in previous work [17] we observe a slight kink in the 1-100 MHz region of the frequency response, which we are currently investigating. We assume the bandwidth response at 100m is similar to that at short distances. From this the -3 dB electrical-electrical (E-E) modulation bandwidth of the devices was recorded, with a maximum of around 960 MHz being achieved (see Fig. 1(d)). However, we observed that the bandwidth gradually decreases to approximately 800 MHz as the current is increased to 20 mA. We tentatively attribute this to the effects of increased current density dependent carrier overflow from the MQWs resulting in increased carrier lifetimes [20]. This is still under investigation, however it has been noted in our other DUV devices and at higher current densities in our UVA devices. The bandwidth measurements are crucial in OWC for optimizing pilot signals and bit loading, as will be discussed in Section 3.

3. DCO-OFDM Setup

3.1 Experimental Setup of the DCO-OFDM Data Link

A UV-enhanced APD (Hamamatsu C56688867) with a bandwidth of 1 GHz, and a nominal responsivity of 7 A/W at 280 nm, was used as a receiver, and an oscilloscope (Keysight MXR608A sampling rate, 16 GSamples/s; analog bandwidth, 6 GHz) captured the received signal for analysis. A laptop was used to generate the digital transmitted signal, analyze the received signal and set the parameters such as the peak-to-peak voltage (VPP). To facilitate the long-distance measurements, the µLED transmitter (Tx) and the receiver (Rx) were placed side-by-side, facing in parallel with a metal sheet placed between them to prevent interference (Fig. 2 shows the view down the optical channel with the metal sheet edge-on in the center). A 5.08 cm×5.08 cm UV-enhanced aluminum mirror (PFSQ20-03-F01) with an average reflectance of approximately 90% was used to reflect the optical signal from the Tx back to the Rx, and this double-pass configuration allowed the total path length to be increased up to 116 m. This mirror was mounted on a Thorlabs Kinematic mount (KM200S) which enabled fine alignment of the mirror. Kinematic mounts were used on the Tx, Rx, and mirror to assist with the alignment of all the optical components where the lenses remained stationary, and the LED and detector were moved ±5 mm to carefully optimize the received signal strength at each distance.

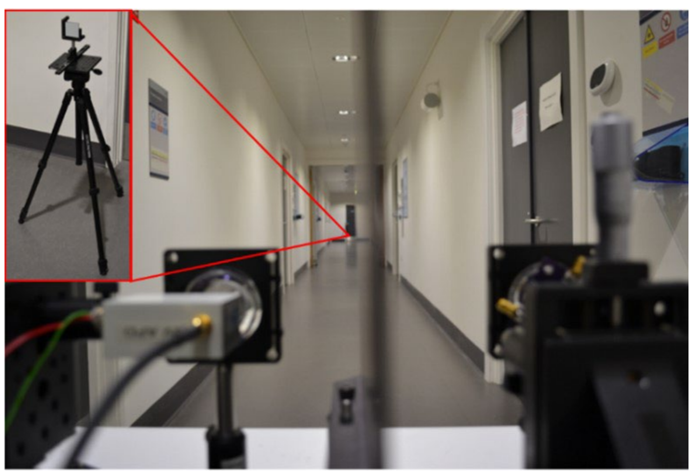

Fig.2. Photographic view of the optical channel, with the micro-LED transmitter on the right and the APD receiver on the left. Inset is a close-up view of the mirror used to retro-reflect the optical signal to increase the path length.

The optical setup used in this work included two 2” diameter fused silica lenses (Edmund Optics 84340 with a numerical aperture of 0.63 and transmittance of 90% at 280 nm) one to collimate the light from the µLED array and the other to focus the returned light onto the receiver. To power the µLEDs, a Yokogawa GS610 power supply was used. For the data transmission, an arbitrary waveform generator (AWG) converts the digital signal to an analog voltage signal (Keysight M8195A, sampling rate 65 GSamples/s; analog bandwidth, 25 GHz;), and the signal from the AWG was amplified (amplifier SHF-S126A), and finally, the RF signal and DC supply were combined using a bias tee (Tektronix PSPL5675A). We use DCO-OFDM for intensity modulation / direct detection (IM/DD) in this work as it allows the use of higher order modulation such as M-QAM (quadrature amplitude modulation), where M denotes the number of constellation points. Moreover, the underlying DCO-OFDM technique can effectively be implemented with digital signal processors (DSPs) [22]. Furthermore, DCO-OFDM, in conjunction with optimum bit and power loading, achieves very high data rates compared to other modulation techniques [23]. The parameters used are shown in Table 1 and were selected with particular care based on empirical optimization guided by theoretical considerations. The implementation steps are shown in Fig. 3. We used DCO-OFDM and applied bit and power loading per subcarrier to maximize the overall data rate given the achieved signal-to-noise ratio (SNR) per subcarrier. This approach enables us to modulate the channel beyond the -3 dB bandwidth of the system. Once the optical alignment was optimized, the bias of the μLED was increased to 20 mA, a bias current that provided an optimal trade-off between increased μLED output power and bandwidth (c.f. Fig. 1.), operating in a relatively linear region of the μLED output power versus voltage response. Moreover, we aimed to select a current value that would not damage the device in the long term. The background lighting was turned off in order to aid alignment.

The VPP was then scanned to pick out the optimum peak-to- peak voltage VPP to use in the experiment to minimize signal clipping and allow us to use the full dynamic range of the μLED. As the transmission distance was increased, the received SNR decreased, primarily due to beam divergence. As a result, the VPP was optimized at each measured distance. Once the VPP was selected, the modulation scheme was applied to a pseudorandom bit stream. The DCO-OFDM time-domain signal clipping level was chosen to be 3.2 times the standard deviation (σ) of the unclipped signal [24] and this enabled us to achieve the highest data rate from the available dynamic range [25]. A Fast Fourier transform (FFT) size of 2048 was used to enable 1023 information-carrying subcarriers. This setting leads to a smaller cyclic prefix to FFT size ratio, which means that the redundant cyclic prefix symbols are transmitted less frequently. The larger FFT size results in increased peak-to-average-power-ratio (PAPR). However, In the experiments, we found that a clipping level of 3.2 achieves a good trade-off between PAPR and nonlinear distortion. The suffix and prefix were used to create a circular convolution between the signal and response so that one-tap equalization is valid and prevents interference between the adjacent OFDM frames. The suffix and prefix lengths are essential to this work as the channel is frequency selective with low pass effects possibly coming from the LED and detector. Single tap frequency domain equalization was used.

Table 1: OFDM parameters used in this work.

Name of Variable	Value of Parameter
Sampling frequency (MHz)	16000
Sample per symbol	5
Symbol span	64
Roll off factor	0.1
FFT Size	2048
Cyclic prefix length	15
Cyclic suffix length	5
Lower clipping	-3.2σ
Upper clipping	3.2σ

In the first stage of implementation (Fig. 3.), a pilot wave was used to assess channel quality, and after this, the bit and power loading was carried out. The data input was initially in a serial form and was changed to parallel channels. *M*-QAM then converts the signal to phase and amplitude. After this, an inverse fast Fourier transform (IFFT) was applied to convert the signal from the frequency domain to the time domain. This result is then converted back to serial for transmission. On the receiver side, a matched filter was used before equalization and data decoding. From this, we compared the received signal vs. the signal transmitted and determined the bit error ratio (BER). We considered forward error correction (FEC) coding with a 7% overhead. Furthermore, we assume a BER threshold of 3.8×10^{-3} for error-free data reception after FEC [24]. When selecting the SNR and Channel gain, multiple adaptive tests were run. Furthermore, we also examined the non-linear (NL) distortion of the µLED and the receiver noise when examining the SNR.

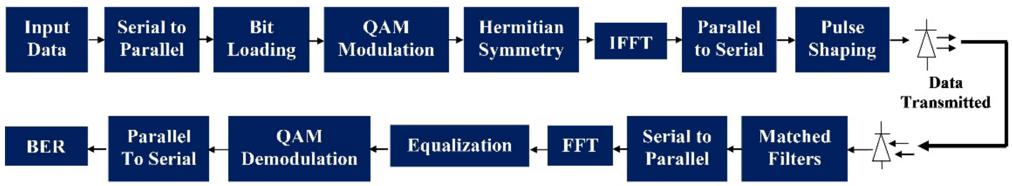

Fig.3. Block diagram of the DCO-OFDM transmission system.

4. Communication Results

4.1 Received power vs. distance

The received optical power focused on the detector is crucial as it determines the SNR and consequently the data rate. The first step in the DCO-OFDM measurement was therefore to examine the power being received by the detector (see Fig. 4.).

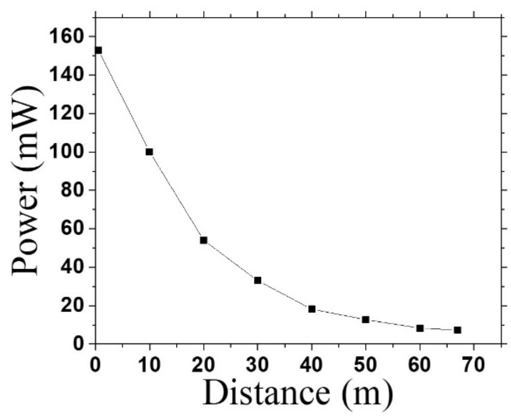

Fig. 4. The received optical power vs. distance, measured with a 300 µm pinhole.

The power was measured using the same power meter used in the L-I measurements, to which a 300 µm pinhole (Thorlabs P300K) was added. This was done in order to reduce the active area of the power meter to the same size as that of the APD. It can be seen in Fig. 4. that the power remains relatively high below 12 m, and only beyond this distance does the intensity of the central spot noticeably decrease, attributed to a combination of beam divergence and the criticality of alignment. After 60 m, we were close to the sensitivity limit of the power meter, so it was not possible to accurately measure the power at greater distances. However, based on the trend data, we assume that the power is on the order of 100s of nanowatts at 116 m. The power measurements were used as a guide to the distances at which we could usefully transmit data.

4.2 Optical communication results

Before transmitting and recording any data, the setup was aligned at each measured distance using a reference sine wave to achieve the optimal SNR (see Fig. 5. (a)). The µLED was biased with 20 mA, this current being selected as described above, and VPP value of the AWG output was adjusted. In Fig. 5. (a) we observe that a low-pass characteristic of the achieved SNR against frequency can be observed. Due to the wide modulation bandwidth of the designed device, the rate of decrease of SNR with frequency is lower compared to commercial broad area LEDs. Moreover, we observe that as the distance increases, the SNR decreases as the signal becomes weaker, primarily due to beam divergence. At these 10's of meter distances, DUV absorption and scattering are not considered to have a significant impact. It is interesting to note that the SNR remains relevantly constant under 10 m (see Fig. 5(a)). To test whether the alignment of the mirror was causing this, we removed the mirror for the 0.5 m set up and used a simple back-to-back bench top set up for reference. However, we saw no improvement in the SNR, which suggests that the data rate may be capped. It is difficult to specify what power would produce a particular data rate, as increases in power do not predictably increase the data rate due to issues such as the nonlinearity of the device, spot size on the detector and noise from the transmitter side, which can cap the SNR and the data rate. However, as the distance increases, the data rate drops rapidly between 10 m – 40 m, although this stabilizes between 40 m – 60 m.

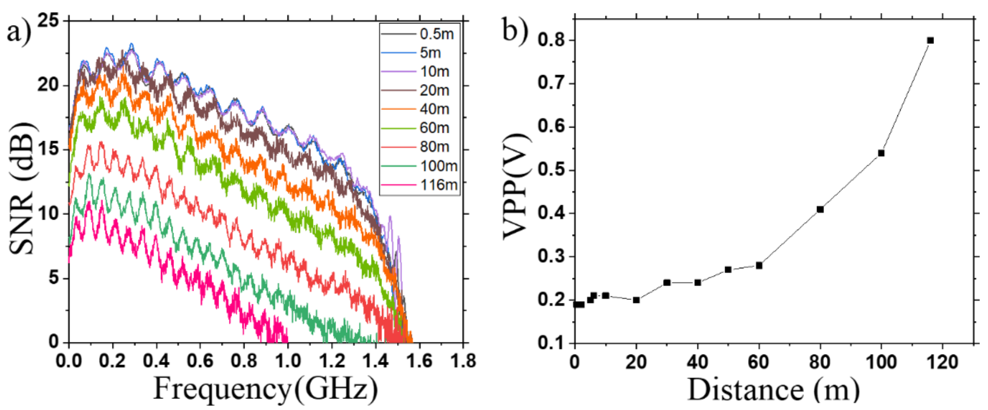

Fig. 5. a) SNR vs. frequency at different distances and b) optimal VPP vs. distance.

The selection of VPP leads to a trade-off between signal strength and NL signal distortion[26]. When applying a greater VPP to the µLED, the optical signal has a higher modulation depth so that the signal strength is boosted. However, the µLED device has a nonlinear behaviour as shown in Fig. 1(a). A greater VPP also means using a greater dynamic range which leads to severer nonlinear distortion. When the link distance is short (under 10 m), the path loss is small, and the SNR is limited by NL distortion. Therefore, a smaller optimal VPP has been found to overcome dominant NL distortion. When the link distance is very large (100 m), the significant optics- and alignment-dependent path loss makes the SNR limited by receiver noise. Therefore, the optimal VPP at these distances is higher. In Fig. 5(b) the optimal VPP supplied by the AWG remains relatively constant around a value of 0.2 V with only minor changes under 20 m. However, as the distance approaches 100 m, the VPP increases rapidly to around 0.5 V. The amplifier has a typical gain of 29 dB and from Fig. 1(a), this gain could put us in a non-linear regime for the device. Furthermore, the ripple features seen in the SNR, as shown in Fig. 5(a), could be a result of impedance mismatch effects between the µLED and drive electronics.

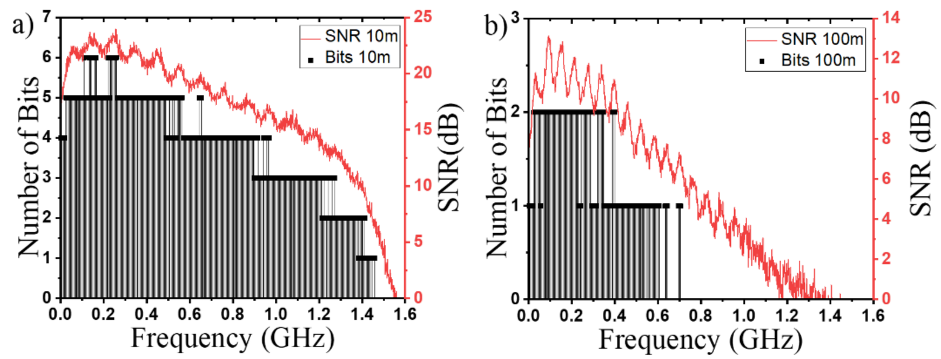

Fig. 6. SNR and bits loaded vs frequency at distances of a) 10m and b) 100m.

The bit loading algorithm is based on the Hughes-Hartogs algorithm[27]. In that approach, using a given amount of transmission energy, it is possible to load as many bits as possible onto the subcarriers and maintain a targeted BER. As a result, this algorithm can maximize the achievable data rate and adapt to various channel conditions. Fig. 6(a) and Fig. 6(b) respectively demonstrate the number of bits loaded at the lowest BER data points at 10 m and 100 m. As Fig. 6(a) shows, 4 or 5 bits could be loaded at shorter distances as the SNR is relatively high. However, as Fig. 6 (b) shows, at approximately 100 m, this dropped to 1 or 2 bits due to the decrease in the SNR. Fig. 6(a) and Fig. 6(b) show that no bit is loaded to subcarriers at SNR lower than approximately 2 dB. Due to the low pass characteristics of the device, fewer bits can be loaded on the high frequency subcarriers. In Fig. 7., we discuss the data rates achieved using this method.

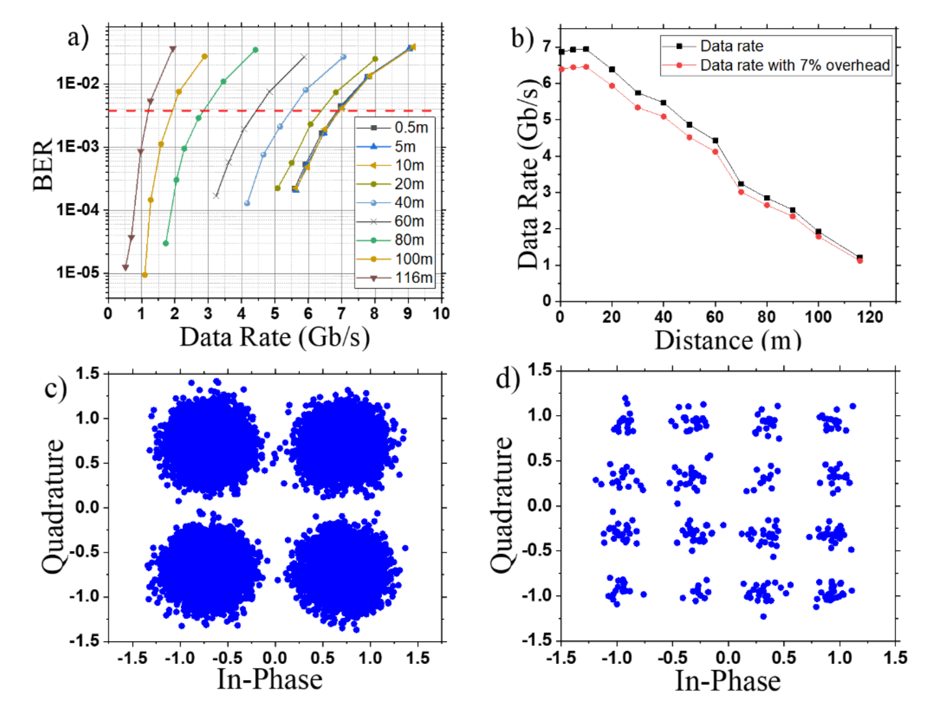

Fig. 7. a) the BER vs. data rate (Dashed line represents a BER of 3.8 x 10^{-3}) b) the data rate vs. distance c) 4-QAM constellation at 70m d) 16-QAM constellation at 70m.

We examined the data rate below a BER of approximately 3.8×10^{-3}, which allows for the application of forward error correction (FEC) (represented by the horizontal dashed line in Fig. 7(a)). Under 10 m, the data rate was relatively constant at greater than 6 Gb/s (see Fig.7(b)) with approximately 6.94 Gb/s achieved (6.45 Gb/s with 7% overhead applied) at 10m. As the distance increases, the data rate decreases approximately linearly as shown in Fig. 7(b), although it is important to note that the VPP was optimized at each distance to attempt to compensate for signal loss due to beam divergence. The maximum link distance of 116 m was limited by the available laboratory corridor space. At this distance, a data rate of approximately 1.20 Gb/s (1.12 Gb/s with 7% overhead applied) was obtained. To the best of our knowledge, this represents the first demonstration of a data rate >1 Gb/s at >100 m using a single DUV µLED, and the longest distance at which 1 Gb/s has been achieved using a µLED of any wavelength. After completing the measurements in a darkened corridor, we repeated the 116 m measurement in ambient light. This had little effect on the data rate, with a data rate of 1.19 Gb/s (1.11Gb/s with 7% correction) at 116m being recorded. The light shielding of the components and their tight and carefully controlled optical alignment may be a factor here. This shows promise for practical free-space communications applications of these devices in such as arena, warehouse, and factory environments.

A detailed study of all the link parameters such as transmitter area, beam divergence angle etc. is beyond the scope of the technology demonstrator shown here. However, long transmission distances were achieved here through careful consideration of the optics used, to ensure sufficient received optical power, guided by modelling of the long-distance link using commercial ray-tracing software (Zemax OpticStudio). A detailed study on the optimisation of device parameters and modulation schemes for optical wireless communication may be found in work by H. Chun et al.[28]. When compared with results from the literature in Fig. 8. [6,7,16,17,29,30], it is evident that this work has demonstrated the possibility of using µLED-based DUV communications for > 100m high data rate applications. We have achieved similar Gb/s data rates but at much greater distances: in some cases, ×10 greater. Several important developments have been implemented to facilitate this. We have improved the fabrication, contacting and operation of the µLED devices, increasing the available (through-sapphire-directed) single-µLED optical output power by a factor of approximately 2.5× from 200 µW [6] to 500 µW. We have also introduced higher numerical aperture optics (using 2-inch lenses here, compared to 1-inch previously).

Furthermore, we have taken particular care over the optical alignment and parameter optimization (including VPP) for the DCO-OFDM protocol, and we have used a receiver with higher bandwidth (1 GHz vs 400 MHz) which has helped in the detection of DUV data rates up to approximately 6.94 Gb/s. We note that the transmission distances demonstrated here were limited by the available laboratory corridor space and not by the intrinsic performance of the system. Even longer transmission distances should thus be achievable, although at increasing distances the effects of atmospheric absorption and scattering will increasingly affect the optical channel. This high data rate line-of-sight (LOS) work, as well as being applicable in its own right, is informing possible NLOS performance improvements for applications such as secure military communications [3].

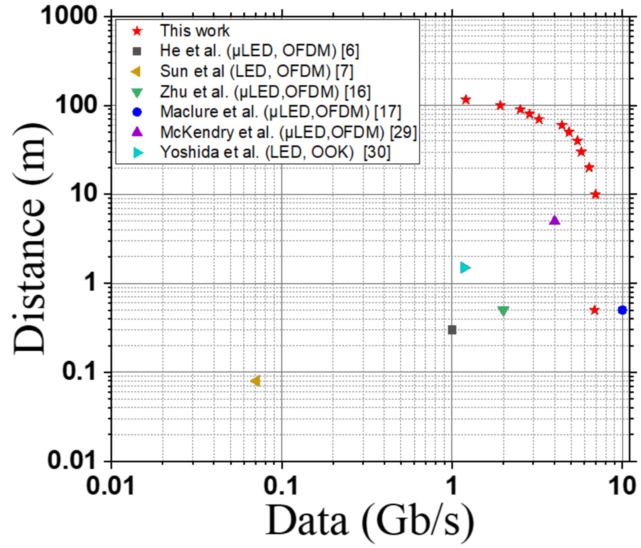

Fig.8. A comparison of the results obtained here to selected previous work in the literature.

5. Conclusion

By careful and detailed optimization of the devices, optical system and communications parameters, we have demonstrated that DUV µLEDs can be used for Gb/s free-space communications at distances of over 100 m in a manner not obviously affected by ambient light. Overall, our results show new optical communication capabilities for DUV µLEDs. Such performance at this distance is a benchmark for OWC application of µLEDs in such practical situations as office environments, lecture theaters, arenas, and warehouses. Furthermore, it gives indications of the potential use of such µLEDs in space-based applications and provides characterization data and design parameters to inform the implementation of high-performance non-line-of-sight communications systems.

Funding

Engineering and Physical Sciences Research Council (EPSRC) (EP/M01326X/1). We acknowledge Fraunhofer UK Research Ltd. for DM's Ph.D. studentship funding.

Acknowledgment

We acknowledge Zhixin Semiconductor Co., Ltd. for the LED wafer material. All authors declare there are no competing financial interests involved in this work.

†These authors contributed equally to this work.

Disclosures

The authors declare no conflicts of interest.

Data Availability

The data are available Ref. [31].

References

1. H. Haas, "LiFi is a paradigm-shifting 5G technology," Reviews in Physics **3**(October 2017), 26–31 (2018).
2. I. K. Son and S. Mao, "A survey of free space optical networks," Digital Communications and Networks **3**(2), 67–77 (2017).
3. D. Moriarty and B. Hombs, "System design of tactical communications with solar blind ultraviolet non line-of-sight systems," MILCOM 2009 - 2009 IEEE Military Communications Conference 1–7 (2009).
4. A. Vavoulas, H. G. Sandalidis, N. D. Chatzidiamantis, Z. Xu, and G. K. Karagiannidis, "A Survey on Ultraviolet C-Band (UV-C) Communications," IEEE Communications Surveys and Tutorials **21**(3), 2111–2133 (2019).
5. T. Y. Aung, S. Arya, and Y. H. Chung, "Performance dependence of non-line-of-sight ultraviolet communications on atmospheric parameters of the ultraviolet channel," Opt Commun **443**(March), 7–11 (2019).
6. X. He, E. Xie, M. S. Islim, A. A. Purwita, J. J. D. McKendry, E. Gu, H. Haas, and M. D. Dawson, "1 Gbps free-space deep-ultraviolet communications based on III-nitride micro-LEDs emitting at 262 nm," Photonics Res **7**(7), B41 (2019).
7. X. Sun, Z. Zhang, A. Chaaban, T. K. Ng, C. Shen, R. Chen, J. Yan, H. Sun, X. Li, J. Wang, J. Li, M.-S. Alouini, and B. S. Ooi, "71-Mbit/s ultraviolet-B LED communication link based on 8-QAM-OFDM modulation," Opt Express **25**(19), 23267 (2017).
8. V. v. Belov, I. Juwiler, N. Blaunstein, M. v. Tarasenkov, and E. S. Poznakharev, "Nlos communication: Theory and experiments in the atmosphere and underwater," Atmosphere (Basel) **11**(10), (2020).
9. D. Han, Y. Liu, K. Zhang, P. Luo, and M. Zhang, "Theoretical and experimental research on diversity reception technology in NLOS UV communication system," Opt Express **20**(14), 15833 (2012).
10. J. Y. Lin and H. X. Jiang, "Development of microLED," Appl Phys Lett **116**(10), 1–8 (2020).
11. J. F. C. Carreira, E. Xie, R. Bian, J. Herrnsdorf, H. Haas, E. Gu, M. J. Strain, and M. D. Dawson, "Gigabit per second visible light communication based on AlGaInP red micro-LED micro-transfer printed onto diamond and glass," Opt Express **28**(8), 12149 (2020).
12. A. D. Griffiths, J. Herrnsdorf, M. J. Strain, and M. D. Dawson, "Scalable visible light communications with a micro-LED array projector and high-speed smartphone camera," Opt Express **27**(11), 15585 (2019).
13. J. J. D. McKendry, R. P. Green, A. E. Kelly, Z. Gong, B. Guilhabert, D. Massoubre, E. Gu, and M. D. Dawson, "High-speed visible light communications using individual pixels in a micro light-emitting diode array," IEEE Photonics Technology Letters **22**(18), 1346–1348 (2010).
14. G.-R. Lin, H.-C. Kuo, C.-H. Cheng, Y.-C. Wu, Y.-M. Huang, F.-J. Liou, and Y.-C. Lee, "Ultrafast 2 × 2 green micro-LED array for optical wireless communication beyond 5 Gbit/s," Photonics Res **9**(10), 2077 (2021).
15. Y. Huang, Z. Guo, H. Huang, and H. Sun, "Influence of Current Density and Capacitance on the Bandwidth of VLC LED," IEEE Photonics Technology Letters **30**(9), 773–776 (2018).
16. S. Zhu, P. Qiu, Z. Qian, X. Shan, Z. Wang, K. Jiang, X. Sun, X. Cui, G. Zhang, D. Li, and P. Tian, "2 Gbps free-space ultraviolet-C communication based on a high-bandwidth micro-LED achieved with pre-equalization," Opt Lett **46**(9), 2147 (2021).
17. D. M. Maclure, J. J. D. McKendry, M. S. Islim, E. Xie, C. Chen, X. Sun, X. Liang, X. Huang, H. Abumarshoud, J. Herrnsdorf, E. Gu, H. Haas, and M. D. Dawson, "10 Gbps wavelength division multiplexing using UV-A, UV-B, and UV-C micro-LEDs," Photonics Res **10**(2), 516 (2022).
18. G. Arvanitakis, R. Bian, J. J. D. Mckendry, and C. Chen, "Gb / s Underwater Wireless Optical Communications Using Series-Connected GaN Micro-LED Arrays," IEEE Photonics J **12**(April), 1–10 (2020).

19. R. X. G. Ferreira, E. Xie, J. J. D. McKendry, S. Rajbhandari, H. Chun, G. Faulkner, S. Watson, D. C. O. Brien, and M. D. Dawson, "High Bandwidth GaN-Based Micro-LEDs for Multi-Gb / s Visible Light Communications," IEEE Photonics Technology Letters **28**(19), 2023–2026 (2016).

20. W. Sun, M. Shatalov, J. Deng, X. Hu, J. Yang, A. Lunev, Y. Bilenko, M. Shur, and R. Gaska, "Efficiency droop in 245-247 nm AlGaN light-emitting diodes with continuous wave 2 mW output power," Appl Phys Lett **96**(6), 245–248 (2010).

21. D. M. Maclure, J. J. D. Mckendry, J. Herrnsdorf, X. He, E. Xie, E. Gu, and M. D. Dawson, "Size-Dependent Characterization of Deep UV Micro-Light- Emitting Diodes," Proceedings of IEEE Conference IPC (1), 2020–2021 (2020).

22. D. Tsonev, S. Sinanovic, and H. Haas, "Complete modeling of nonlinear distortion in OFDM-based optical wireless communication," Journal of Lightwave Technology **31**(18), 3064–3076 (2013).

23. D. Tsonev, S. Videv, and H. Haas, "Unlocking Spectral Efficiency in Intensity Modulation and Direct Detection Systems," IEEE Journal on Selected Areas in Communications **33**(9), 1758–1770 (2015).

24. M. S. Islim, R. X. Ferreira, X. He, E. Xie, S. Videv, S. Viola, S. Watson, N. Bamiedakis, R. v. Penty, I. H. White, A. E. Kelly, E. Gu, H. Haas, and M. D. Dawson, "Towards 10 Gb/s orthogonal frequency division multiplexing-based visible light communication using a GaN violet micro-LED," Photonics Res **5**(2), A35 (2017).

25. D. Tsonev, H. Chun, S. Rajbhandari, J. J. D. McKendry, S. Videv, E. Gu, M. Haji, S. Watson, A. E. Kelly, G. Faulkner, M. D. Dawson, H. Haas, and D. O'Brien, "A 3-Gb/s single-LED OFDM-based wireless VLC link using a gallium nitride μ LED," IEEE Photonics Technology Letters **26**(7), 637–640 (2014).

26. S. Dimitrov and H. Haas, "Information rate of OFDM-based optical wireless communication systems with nonlinear distortion," Journal of Lightwave Technology **31**(6), 918–929 (2013).

27. D. Hughes-Hartogs, "Ensemble modem structure for imperfect transmission media.," (1986). U.S. Patent No. 4679227, July 1987; 4731816, March 1988; 4833706, May 1989.

28. H. Chun, S. Rajbhandari, G. Faulkner, E. Xie, J. J. D. Mckendry, E. Gu, M. D. Dawson, and D. O'Brien, "Optimum Device and Modulation Scheme Selection for Optical Wireless Communications," Journal of Lightwave Technology **39**(8), 2281–2287 (2021).

29. J. J. D. McKendry, E. Xie, M. S. Islim, X. Sun, D. MacLure, E. Gu, H. Haas, and M. D. Dawson, "4 Gbps wireless optical communications up to 5 m using a UV-C micro-light-emitting diode array," 2021 IEEE Photonics Conference, IPC 2021 - Proceedings **1**, 2022–2023 (2021).

30. Y. Yoshida, K. Kojima, M. Shiraiwa, Y. Awaji, A. Kanno, N. Yamamoto, S. F. Chichibu, A. Hirano, and M. Ippommatsu, "An Outdoor evaluation of 1-gbps optical wireless communication using algan-based led in 280-nm band," 2019 Conference on Lasers and Electro-Optics, CLEO 2019 - Proceedings **5–6** (2019).

31. https://doi.org/10.15129/ea008020-bd2f-466a-bd53-ec31f74901eb